Available online at www.sciencedirect.com
SCIENCE DIRECT®
Catalysis Today 98 (2004) 131–139
CATALYSIS TODAY
www.elsevier.com/locate/cattod

Highly active MoS_2 on wide-pore ZrO_2–TiO_2 mixed oxides

M.C. Barrera[a,b], M. Viniegra[a,*], J. Escobar[c,*], M. Vrinat[d], J.A. de los Reyes[b], F. Murrieta[c], J. García[b]

[a]*Depto. de Química, Universidad Autónoma Metropolitana-Iztapalapa, San Rafael Atlixco 186, Col. Vicentina, Iztapalapa, 09340 México, D.F., México*
[b]*Depto. de Area de Ing. Química, Universidad Autónoma Metropolitana-Iztapalapa, San Rafael Atlixco 186, Col. Vicentina, Iztapalapa, 09340 México, D.F., México*
[c]*Instituto Mexicano del Petróleo, Tratamiento de Crudo Maya, Eje Central Lázaro Cárdenas 152, San Bartolo Atepehuacan, G.A. Madero, 07730 México, D.F., México*
[d]*Institut de Recherches sur la Catalyse, CNRS, 2 Av. A. Einstein, 69626 Villeurbanne, France*

Abstract

Wide-pore ZrO_2–TiO_2 (Zr/Ti = 30/70) was prepared by low-temperature (273 K) sol–gel technique followed by solvo-treatment. Higher surface area ($S_g \sim 340$ m^2 g^{-1}) and porosity ($V_p \sim 0.8$ cm^3 g^{-1}) were registered after solvo-treatment at 353 K (1 day) for samples calcined at 773 K. Wider pores (∼22 nm) but much lower S_g (∼80 m^2 g^{-1}) were observed when solvo-treatment was carried out at 513 K. Even larger pores with almost no additional S_g decrease were obtained by prolonging that stage. MoS_2 catalysts supported on binary oxides solvo-treated at 353 K showed increased intrinsic activity (by a factor of ∼3.3) in dibenzothiophene hydrodesulfurization (593 K and 5.6 MPa), as to that impregnated on conventional ZrO_2–TiO_2 (at 2.8 Mo atoms nm^{-2}). By itself, Mo sulfidability (as determined by XPS) seemed not to dictate the activity trends found. Surface Lewis acidity appeared to play a decisive role on HDS performance, probably by influencing both Mo sulfidability and dispersion. Highly-loaded catalysts (5.6 Mo atoms nm^{-2}) had decreased activity, probably due to lower MoS_2 dispersion. Additional characterization comprised chemical analysis (ICP), XRD, thermal analysis, acidity measurements (by pyridine FTIR) and UV–vis DRS. Tailoring ZrO_2–TiO_2 texture, traditionally characterized by narrow micro-mesoporosity results promising in developing novel hydrotreating catalyst supports.

Keywords: Zirconia–Titania; Sol–Gel; Solvo-thermal treatment; Hydrodesulfurization

1. Introduction

ZrO_2–TiO_2 mixed oxide systems have shown interesting properties as catalyst and catalyst support [1–3]. In particular, they have recently attracted attention in hydrotreating (HDT) schemes [4–5] and high surface area materials could be obtained at certain compositions. However, their low porosity and reduced pore diameter (3–4 nm) constitute an important drawback that limits their potential practical applications [4–6]. To overcome these constraints, some efforts have been focused in improving textural properties by various synthesis methodologies [6–9]. For instance, some good results have been obtained by pH–swing precipitation (materials calcined at 623 K) [7], although detailed characterization of final mixed oxides is lacking. Another possibility could be to prepare highly porous aerogels [10] but low stability under hydrodesulfurization (HDS) reaction conditions of super-critically-dried ZrO_2–TiO_2 has precluded its extended utilization [9]. On the other hand, solvo-thermal post-treatments during sol–gel processing could be useful to improve textural properties of mixed oxides. For instance, solvo-thermally treated Al_2O_3-modified ZrO_2 of higher surface area and pore volume than samples synthesized by CO_2 super-critical drying has been prepared [11], the best results being attained with an ethanol–water mixture. Our group has recently reported the feasibility of improving ZrO_2–TiO_2 texture by solvo-thermal post-treatments during sol–gel synthesis [12]. At our best

* Corresponding author.
E-mail addresses: mvr@xanum.uam.mx (M. Viniegra), jeaguila@imp.mx (J. Escobar).

0920-5861/$ – see front matter © 2004 Elsevier B.V. All rights reserved.
doi:10.1016/j.cattod.2004.07.027

knowledge, that has been the only published application of that methodology to produce wide-pore zirconia–titania. In the past, hydrothermal methods have been applied to prepare nanosized TiO_2 and to determine its influence on phase evolution [13–17]. Synthesis of nanosized ZrO_2 has also been tried by using hydrothermal techniques [13]. In all those cases, however, the effect of operating conditions on textural properties of final materials has been rarely addressed and the corresponding pore size distributions have not even been reported.

Regarding the HDS catalysts requirements, high pore volume could influence Mo dispersion by using less concentrated solutions during impregnation to get a given target loading. Also, wider pores could facilitate diffusion of hydrocarbons constituting middle distillates at HDT conditions. Even more, there is the possibility of avoiding rapid deactivation due to pore-plugging by carbonaceous deposits, as indeed observed in thiophene HDS over $CoMo/TiO_2$–ZrO_2 catalysts with pores in the 4–4.5 nm range [6].

Hereby, we undertook a detailed characterization of solvo-thermally treated ZrO_2–TiO_2 by applying N_2 physisorption, X-ray diffraction (XRD), thermal analysis, acidity measurements (by pyridine FTIR), UV–vis DRS and XPS. In order to evaluate the influence of improved textural properties on HDS activity of ZrO_2–TiO_2-supported MoS_2 catalysts, binary oxides were impregnated at different Mo loadings by incipient wetness and tested in the liquid-phase dibenzothiophene hydrodesulfurization at conditions close to those used in industrial facilities. Coordination state of oxidic impregnated Mo was determined by UV–vis DRS meanwhile Mo oxidation state after sulfiding was determined by XPS.

2. Experimental

2.1. Materials

Wide-pore ZrO_2–TiO_2 mixed oxides (Zr/Ti = 30/70 nominal molar ratio) were synthesized by low-temperature sol–gel method followed by solvo-thermal treatment [12]. That composition was chosen to prepare mixed oxides of maximized surface area [18]. Zr(IV) propoxide and Ti(IV) isopropoxide (both from Aldrich) were diluted in isopropanol (ROH, Baker). A de-ionized H_2O + HNO_3 (Baker) mixture was drop-wise added to the alkoxides solution kept under vigorous stirring at ~273 K (T_s). The ROH/alk., H_2O/alk. and HNO_3/alk. mol ratios used were 65, 20 and 0.05, respectively. After alkoxide hydrolysis, the alcogels submerged in the mother liquor were submitted to post-treatments at different conditions (353 or 513 K for 1 or 4 days) in a stainless steel hermetic autoclave (Parr 4560) under autogenic pressure. After this stage, the materials were vacuum-dried until total solvent elimination, treated at 393 K (2 h) and finally calcined at various temperatures (773–973 K, 4 h) under static air atmosphere. As reference, a sample aged in the mother liquor (1 day at 273 K, no solvo-thermal treatment) was also prepared. Further processing comprised drying and annealing under similar conditions than the rest of solids.

Supports calcined at 773 K were impregnated at incipient wetness with $(NH_4)_6Mo_7O_{24}{\cdot}4H_2O$ (Aldrich) at 2.8 Mo atoms nm^{-2}. Higher loading (5.6 Mo atoms nm^{-2}) was also tried for supports solvo-treated at 353 K. The impregnated materials were dried at 393 K (2 h) after aging at room temperature (overnight) then calcined at 673 K (4 h) under static air atmosphere. The final catalysts were obtained by sulfiding at 673 K (1 h) under a H_2S/H_2 stream (Praxair, 10 vol.%, 4 L h^{-1}).

2.2. Materials characterization

N_2 physisorption at 77 K (Autosorb Quantachrome) was used for textural characterization. Structural order was studied by XRD (Siemens D-500 Kristalloflex, $Cu_{K\alpha}$ radiation, λ = 0.15406 nm). Thermal analyses were carried out with a Netzch Thermische Analize, STA 409 EP apparatus under static air atmosphere. Supports surface acidity (T_c = 773 K) was analyzed by pyridine thermo-desorption studied in the infrared region (Fourier Transform Infrared Nicolet 710 spectrophotometer) in the 473–773 K temperature range. Chemical analysis of Mo impregnated mixed oxides was carried out by AES–ICP (atomic emission spectroscopy-inductively coupled plasma) using a SPECTROFLAME-ICP model D (Spectro). Mo^{6+} coordination in calcined impregnated precursors (T_c = 673 K) was studied by diffuse reflectance spectroscopy (Varian Cary 5E UV–vis-NIR spectrophotometer, praying mantis attachment). $BaSO_4$ (Kodak) was used as white reflectance standard to obtain a baseline at 298 K.

Selected samples of sulfided catalysts were analyzed by XPS. The spectra were recorded with a VG Scientific Escalab 200R spectrometer equipped with $Mg_{K\alpha}$ X-ray source and a hemispherical analyzer. Experimental peaks were decomposed into components using mixed Gaussian–Lorentzian functions and a non-linear squares fitting algorithm. Shirley background subtraction was applied. An intensity ratio of 2/3 and a splitting of 3.2 eV were used to fit the Mo 3d peaks. Surface composition was determined from the integrated peaks of Mo 3d, Zr 3d and Ti 2p using their respective experimental sensitivity factors. Binding energies were reproducible to within ±0.2 eV and the C 1s peak at 284.5 eV was used as reference.

2.3. DBT HDS reaction test

Sulfided catalysts were tested in dibenzothiophene (DBT, Aldrich) hydrodesulfurization (HDS) in a tri-phasic batch reactor (Parr 4562 M), using *n*-hexadecane (Aldrich) as solvent. Operating conditions (carefully chosen to avoid external and/or internal diffusional limitations) were P_{H_2} = 5.59 ± 0.03 MPa, T_R = 593 ± 2 K and 1000 RPM (~105 rad s^{-1}) mixing speed. Samples taken periodically

were analyzed in a gas chromatograph Perkin-Elmer AutoSystem XL (flame ionization detector and Ultra 2 capillary column, crosslinked 5% Ph Me Silicone phase). HDS kinetic constants were calculated assuming pseudo-first-order kinetics referred to DBT concentration (x = conversion, t = time):

$$k = \frac{-\ln(1-x)}{t} \quad (1)$$

k values were normalized by considering reaction volume and mass of catalyst used (k expressed in $m^3\ kg_{cat.}^{-1}\ s^{-1}$).

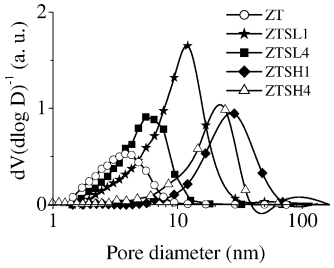

Fig. 1. Effect of solvo-thermal treatment under various conditions on the pore size distribution of sol–gel ZrO_2–TiO_2 (Zr/Ti = 30/70 nominal molar ratio) samples (T_c = 773 K) from [12].

3. Results and discussion

3.1. Supports characterization

The surface area (S_g), pore volume (V_p) and mean pore diameter (D_p) of mixed oxides prepared under various conditions are presented in Table 1. After annealing at any temperature, the solids prepared by low-temperature solvo-thermal method (ZTSL1 and ZTSL4 series) showed improved values of all those textural parameters, as compared with the solid aged in the mother liquor (ZT). Conversely, after high-temperature solvo-treatment materials of much lower surface area were obtained (ZTSH series). Although the S_g of ZTSL1 was larger (~1.9 times) than that of ZTSL4 (dried samples) both solids showed similar values after annealing at more severe conditions ($T \geq 773$ K). Increased pore volume was registered for solvo-treated materials, the V_p of ZTSL1 being more than three-fold to that of ZT (samples at T_c = 773 K). As previously reported [19], the ZT sample calcined at 773 K showed pore size distribution (PSD) centered in the microporous-mesoporous boundary region (Fig. 1), similar to those reported for zirconia–titania prepared through various methods [20,21]. On the other hand, a notable increase in pore diameter was registered for ZTSL1. By prolonging the low-temperature solvo-treatment the shape of the corresponding N_2 physisorption isotherms (solids at T_c = 773 K, not shown) notably changed. ZTSL1 showed type IV adsorption branch (BDDT classification) but that solvo-treated at similar temperature for longer time (ZTSL4) had much more pronounced hysteresis loop (type E, de Boer classification) suggesting ink-bottle pores, probably formed by agglomeration of small spherical particles. These modifications were reflected in strongly decreased porosity and PSD shifted to lower diameters (maximum at ~6 nm, Fig. 1). Drying time (under vacuum) strongly influenced the porosity and pore size of materials. By increasing its duration, mixed oxides of lower porosity and decreased pore

Table 1
Effect of solvo-thermal treatment under various conditions on textural properties of ZrO_2–TiO_2 (Zr/Ti = 30/70 nominal molar ratio) materials dried (393 K) or calcined (773–973 K)

Support	Aging T (K)	Aging time (days)	T_c[a] (K)	S_g[b] ($m^2\ g^{-1}$)	V_p[c] ($cm^3\ g^{-1}$)	D_p[d] (nm)
ZT	273	1	393	482	0.36	3.0
			773	290	0.25	3.5
			973	57	0.19	13.5
ZTSL1	353	1	393	603	1.10	7.1
			773	338	0.80	8.9
			973	69	0.55	32.0
ZTSL4	353	4	393	319	0.40	5.1
			773	316	0.40	5.1
			973	73	0.32	18.0
ZTSH1	513	1	393	96	0.46	19.3
			773	83	0.46	22.3
			973	50	0.45	36.0
ZTSH4	513	4	393	72	0.43	24.0
			773	70	0.44	25.0
			973	60	0.40	29.0

Some of these results previously presented in [12].
[a] Calcination temperature.
[b] BET surface area.
[c] Pore volume.
[d] Mean pore diameter from $4 \times (V_p/S_g)$.

diameters were observed (not shown) probably due to the continuation of poly-condensation reactions and coarsening phenomena in the mother liquor still present [22]. ZT presented N_2 adsorption isotherm similar to that of ZTSL4 but the hysteresis loop shifted to lower relative pressure, the pattern resembling that previously reported [21] for equimolar sol–gel zirconia–titania (T_c = 773 K).

Wider pores were observed after high-temperature solvo-treatment (ZTSH1 solids) although a four-fold decrease in S_g as to that of ZTSL1 was also registered (samples at T_c = 773 K, Table 1). Even larger pores were obtained by prolonging the high-temperature solvo-thermal treatment with almost no additional surface area decrease (Fig. 1 and Table 1). Thus, it was demonstrated that by varying temperature and duration of solvo-thermal treatment ZrO_2–TiO_2 materials of tailor-made pore distributions could be prepared.

As expected [19], the formerly amorphous ZT material crystallized to $ZrTiO_4$ after calcination at 973 K (Fig. 2), the excess TiO_2 being dissolved in the zirconate matrix [23]. The low-temperature solvo-thermal treatment did not affect that behaviour (samples ZTSL, not shown). On the other hand, the dried ZTSH solids were constituted by separated domains of well-crystallized anatase TiO_2 and a mixture of microcrystalline monoclinic and tetragonal ZrO_2 (Fig. 3). The structure remained unaltered after calcination at severe conditions (T_c = 773–973 K). The anatase to rutile phase change delay could be related to stabilization of titania matrix by solid solution with ZrO_2. Similarly, zirconia crystallization would be impeded by TiO_2 in the solid matrix. Segregation to titania and zirconia single phases doped with the second oxide has been reported for ZrO_2–TiO_2 of similar composition, when submitted to hydro-thermal treatment at severe conditions [24].

From DTA analyses of ZT and ZTSL materials, exothermal signals that could be originated in combustion of alkoxy groups still retained in the solid matrix were observed at ∼550–760 K (Fig. 4). This fact suggested partial hydrolysis of organic precursors at the low-temperature (273 K) synthesis conditions and incomplete condensation reactions. The higher weight loss of ZT respecting to ZTSL samples in the 403–533 K range (thermogravimetrical analyses, not shown) seemed to be due to more incomplete condensation during aging in the mother liquor. On the other hand, for ZTSH samples exothermal peaks attributable to organics combustion were almost absent indicating nearly complete alkoxy ligands removal, in agreement with the very small weight loss in the aforementioned temperature range. Almost total organic remains elimination would promote formation of more metal–O–metal bonds, then facilitating crystal growing [17]. The exothermal inflection (at ∼980 K) related to crystallization to $ZrTiO_4$ [6,23] was not observed for ZTSH solids composed of segregated zirconia–titania domains (Fig. 3). By different mechanisms, crystal growth could be facilitated under high-temperature solvo-treatment resulting in partially sintered materials of moderate S_g but large pores.

Regarding surface acidity of materials calcined at 773 K, ZT did not present Brønsted sites (Fig. 5) that could promote cracking or isomerization reactions [25]. Even more, this sample exhibited very small amounts of Lewis acid centers that could retain pyridine at temperatures up to 573 K (medium acidity). This fact was opposite to that reported in the past for ZrO_2–TiO_2 oxides where surface acidity could be created by strong interaction between components [6,9]. These apparently contradictory results could be rationalized considering that in [6] supports were calcined at 623 K where a less de-hydroxylated surface could present some Brønsted acidity, as reported by Lahousse et al. [18]. In the same line, Zou and Lin [26] identified just terminal OH groups on sol–gel zirconia–titania calcined at 723 K. After more severe annealing, those groups disappeared. In agreement with our results, Barthos et al. [27] did not

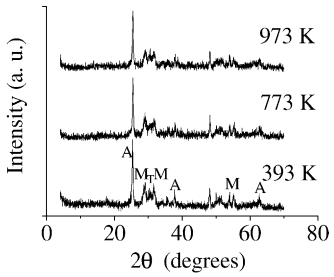

Fig. 3. Structural phase evolution of sol–gel ZrO_2–TiO_2 (Zr/Ti = 30/70 nominal molar ratio) solvo-treated at 513 K (4 days). A: TiO_2 anatase, M: monoclinic ZrO_2, T: tetragonal ZrO_2.

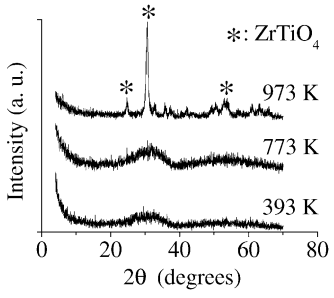

Fig. 2. Structural phase evolution of sol–gel ZrO_2–TiO_2 (Zr/Ti = 30/70 nominal molar ratio) aged in the mother liquor.

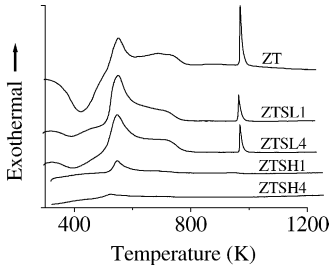

Fig. 4. Differential thermal analysis of sol–gel ZrO_2–TiO_2 (Zr/Ti = 30/70 nominal molar ratio) dried precursors.

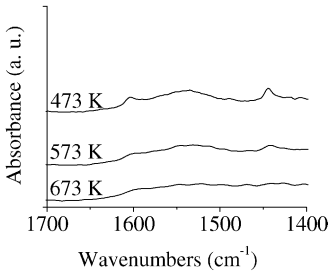

Fig. 5. FTIR spectra of pyridine adsorbed at different temperatures on non-solvo-treated sol–gel ZrO_2–TiO_2 (Zr/Ti = 30/70 nominal molar ratio) (T_c = 773 K).

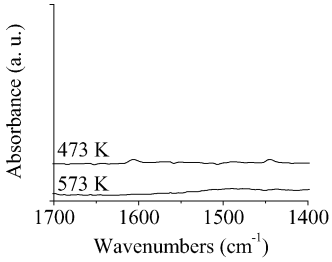

Fig. 7. FTIR spectra of pyridine adsorbed at different temperatures on sol–gel ZrO_2–TiO_2 (Zr/Ti = 30/70 nominal molar ratio) solvo-treated at 513 K (1 day) (T_c = 773 K).

observe protonic acid on ZrO_2–TiO_2 calcined at higher temperature (823 K).

ZTSL solids showed much higher medium-strong Lewis acidity. Again, no Brønsted sites were registered, Fig. 6. Conversely, surface acidity was almost totally absent for ZTSH1 (Fig. 7). In Table 2, a quantification of acid sites density is shown. Increased density of Lewis sites in ZTSL1 and ZTSL4 is clearly evident. These profound changes in acidity imply deep modifications on mixed oxides surface properties due to solvo-thermal synthesis. Zhou and Lin [26] found deep changes in acidity on sol–gel ZrO_2–TiO_2 as function of composition. According to this, strong effects on surface composition by solvo-treatment at various conditions could be envisaged.

UV–vis DRS spectra of supports calcined at 773 K are shown in Fig. 8. In order to have basis of comparison, those of TiO_2 and ZrO_2 single oxides prepared through a similar technique (excepting solvo-treatment) are also included. Pure zirconia presented typical high-energy maximum in the 204–209 nm range related to full connectivity of Zr–O–Zr linkages [28]. Meanwhile, the maximum of titania absorption located at 350–360 nm could be attributed to isolated Ti^{4+} sites in octahedral coordination [29]. Intermediate bands registered for binary oxides could be primarily interpreted as evidence of the existence of mixed matrices [28]. For solvo-thermally treated samples a blue-shifted onset of the low-energy edge was observed as to that of ZT, this phenomenon being more pronounced for ZTSL oxides. Again, this would suggest important differences in the properties of the mixed oxides obtained through solvo-treatments. The ZTSH solids presented more intense high-energy absorption (resembling that of zirconia) and incipient formation of the typical titania absorption band, in agreement with the presence of separated ZrO_2 and TiO_2 domains (Fig. 3). Nevertheless, the absence of definite bands associated to those oxides would confirm that, in spite of segregation, no pure single phases existed but rather titania-rich and zirconia-rich solid solutions.

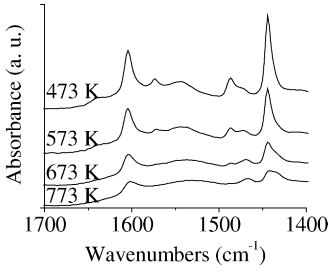

Fig. 6. FTIR spectra of pyridine adsorbed at different temperatures on sol–gel ZrO_2–TiO_2 (Zr/Ti = 30/70 nominal molar ratio) solvo-treated at 353 K (4 days) (T_c = 773 K).

3.2. Impregnated precursors characterization

The UV–vis DRS spectra of ZTSL1-supported materials, representing the common pattern found for the Mo/ZT and Mo/ZTSL oxidic impregnated precursors, are shown in Fig. 9. Signals corresponding to Mo^{6+} oxospecies in tetrahedral (250–280 nm) and octahedral (290–390 nm) coordination [30] could be merged with the broad band corresponding to support (ZTSL1) absorption (maximum at 200–300 nm, Fig. 8). By increasing Mo loading, the low-energy absorption edge red-shifted probably due to formation of species of higher coordination state [31], then, of lower dispersion. Also, the proportion of octahedral Mo^{6+} appeared to increase in the sample of higher Mo concentration.

For the ZTSH1-supported samples (not shown), the onset of Mo oxo-species absorption band coincided with that of the segregated binary oxide. This could convert the oxidic Mo/ZTSH systems in semiconductors where the different Mo oxide centers were in electronic contact with one another and with the Ti^{6+} cations through the conduction band, as recently proposed by Ramírez et al. [32] regarding titania-supported Mo species.

Table 2
Quantification of Lewis surface acid sites (by pyridine thermo-desorption) on ZrO_2–TiO_2 (Zr/Ti = 30/70 nominal molar ratio) materials calcined at 773 K

Sample	Lewis acidity ($\times 10^{-8}$ $mol_{pyridine}$ m^{-2})		
	473 K[a]	573 K[a]	673 K[a]
ZT	20	9	0
ZTSL1	96	43	0
ZTSL4	98	49	24
ZTSH1	25	0	0

[a] Desorption temperature.

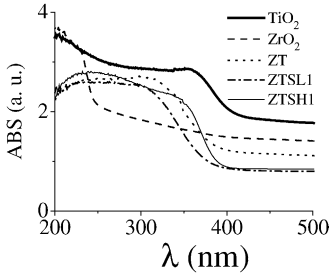

Fig. 8. UV–vis DRS spectra of sol–gel ZrO_2, TiO_2 and their corresponding mixed oxides (Zr/Ti = 30/70 nominal molar ratio) (T_c = 773 K).

3.3. DBT HDS activity test

The ZTSL-supported catalysts of lower Mo loading showed the highest activity among all the solids studied (Table 3). The improvement in HDS performance by solvo-treatment at 353 K was specially notable for Mo(2.8)/ZTSL4 where increased strength of Lewis acidity could influence MoS_2 dispersion [33]. By contrast, although initially very active, the ZTSH-supported catalysts were rapidly deactivated under reaction conditions (Fig. 10). So far, we do not have a satisfactory explanation to that phenomenon. To get insight in sulfided phase dispersion, XRD analyses were carried out for all tested catalysts. No diffraction lines attributable to MoS_2 were registered in any case. This would imply high active phase dispersion for all materials. Moreover, it would suggest that sintering under reaction conditions could be responsible for rapid deactivation of ZTSH-supported catalysts. Indeed, Xu et al. [34] found very similar deactivation phenomena for well-dispersed catalysts tested in dibenzothiophenic compounds HDS. After performing High-Resolution TEM characterization of spent deactivated catalysts, those authors attributed deactivation under reaction conditions to the marked sintering observed. Thus, it could be that the ZTSH supports surface inertness originated in their practically total acidity absence would result in very weak interaction with the supported MoS_2 which would become then prone to sintering. However, extensive characterization of spent catalysts is needed to confirm this assumption.

Taking into account the differences in both surface area of the supports and Mo loading in catalysts, the intrinsic HDS reaction rate is a better basis of comparison (Fig. 11). For Mo(2.8) materials the trends are alike to that previously observed (Table 3). However, for both Mo(5.6) catalyst a notably decreased activity slightly lower to that of the ZT-supported solid is now evident. Conversely to TiO_2 where high amounts of molybdenum could be effectively dispersed producing catalyst of improved HDS properties [35], increasing Mo concentration in ZTSL-supported solids resulted detrimental, probably due to less-dispersed larger MoS_2 crystals formation. As previously mentioned, however, XRD analysis of highly-loaded Mo catalysts failed to provide valuable information. It could not be discarded that highly-disordered MoS_2 particles could remain undetectable by the technique used. In agreement with our findings, the optimum Mo concentration on HDS catalyst supported on

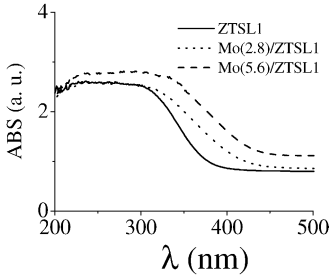

Fig. 9. UV–vis DRS spectra of oxidic impregnated Mo on ZrO_2–TiO_2 (Zr/Ti = 30/70 nominal molar ratio) solvo-treated at 353 K (1 day), (T_c = 673 K), at different Mo loadings.

Table 3
Pseudo first order kinetic constants (DBT HDS) promoted by various MoS_2 catalysts supported on ZrO_2–TiO_2 (Zr/Ti = 30/70 nominal molar ratio) oxides

Sample	$k \times 10^6$ ($m^3\ kg_{cat}^{-1}\ s^{-1}$)
Mo(2.8)/ZT	2.47
Mo(2.8)/ZTSL1	6.45
Mo(5.6)/ZTSL1	4.25
Mo(2.8)/ZTSL4	7.82
Mo(5.6)/ZTSL4	3.44
Mo(2.8)/ZTSH1	Very rapidly deactivated
Mo(2.8)/ZTSH4	Very rapidly deactivated

P_{H_2} = 5.59 ± 0.03 MPa, T_R = 593 K, mixing speed: 1000 RPM (∼105 rad s^{-1}), solvent: *n*-hexadecane.

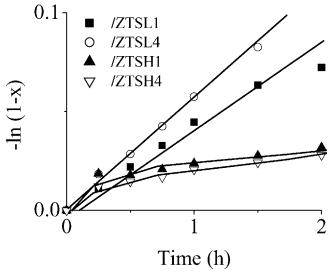

Fig. 10. Pseudo first order reaction rate plots (DBT HDS) of MoS_2 catalysts (2.8 Mo atoms nm^{-2}) supported on solvo-treated ZrO_2–TiO_2 (30/70 nominal mol ratio). P_{H_2}= 5.59 ± 0.03 MPa, T_R = 593 ± 2 K, 1000 RPM (∼105 rad s^{-1}) mixing speed, solvent: *n*-hexadecane.

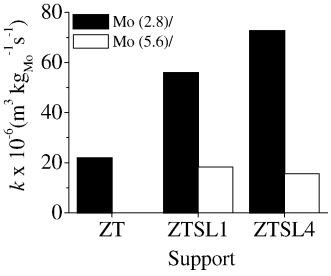

Fig. 11. Pseudo first order intrinsic kinetic constants (DBT HDS) promoted by MoS_2 supported on ZrO_2–TiO_2 (Zr/Ti = 30/70 nominal molar ratio) oxides. P_{H_2}= 5.59 ± 0.03 MPa, T_R = 593 ± 2 K, 1000 RPM (∼105 rad s^{-1}) mixing speed, solvent: *n*-hexadecane.

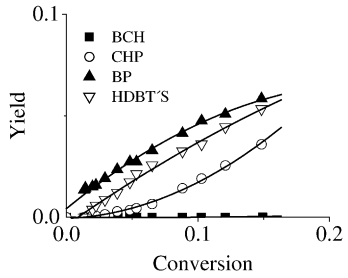

Fig. 12. Selectivity pattern (DBT HDS) for sulfided Mo(2.8) on non-solvotreated ZrO_2–TiO_2 (Zr/Ti = 30/70 nominal molar ratio). P_{H_2}= 5.59 ± 0.03 MPa, T_R = 593 ± 2 K, 1000 RPM (∼105 rad s^{-1}) mixing speed, solvent: *n*-hexadecane.

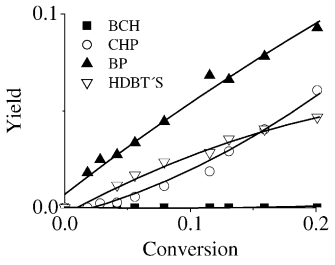

Fig. 13. Selectivity pattern (DBT HDS) of sulfided Mo(2.8) on ZrO_2–TiO_2 (Zr/Ti = 30/70 nominal molar ratio) solvo-treated at 353 K (4 days). P_{H_2} = 5.59 ± 0.03 MPa, T_R = 593 ± 2 K, 1000 RPM (∼105 rad s^{-1}) mixing speed, solvent: *n*-hexadecane.

ternary oxides ZrO_2–TiO_2–V_2O_5 was much lower to that of TiO_2-supported materials [25].

The DBT HDS selectivity pattern found for Mo(2.8)/ZT (Fig. 12) changed for the catalysts supported on ZTSL oxides (Fig. 13). For the latter, no effect of either Mo loading or solvo-treatment duration on products distribution was registered. ZTSH-supported materials were not taken into account in this comparison because their rapid deactivation would complicate to accurately determine their selectivity. Direct desulfurization (DDS) to biphenyl (BP) [36] was favored over all materials, but the BP/hydroDBT ratio was lower for Mo(2.8)/ZT. On the other hand, the cyclohexylphenyl (CHP) proportion remained unaltered. According to the ''rim-edge'' model proposed by Daage and Chianelli [37] that could be indicative of differences in stacking degree of MoS_2 supported particles, crystallites composed of lower number of stacked layers favoring the hydrogenation route (HYD) to hydroDBT's [36]. Other authors [38] proposed that DDS/HYD selectivity depends on various other factors, namely distribution of the primary dihydrointermediates, hydrogen availability on the catalytic centers on which they adsorb and basicity of the S anions associated to catalytic centers.

Considering that BP hydrogenation to CHP could be strongly inhibited by DBT competitive adsorption under our HDS conditions [39], the constant proportion of cyclohexylphenyl over various catalysts would indicate that although HYD route [37] was slightly increased over Mo(2.8)/ZT its hydroDBT's desulfurization rate was lower.

3.4. Sulfided catalysts characterization

Bulk (by ICP) and surface (by XPS) analyses were applied to characterize selected sulfided catalysts composition, Table 4. Molybdenum content fairly agreed with that intended during incipient impregnation. In the same line, Zr/Ti bulk ratio could be considered as among experimental error. On the other hand, ZrO_2-rich surface was determined for Mo(2.8)/ZT. Similar results have been observed for equimolar zirconia–titania prepared by different methods, the strongest effect being found for mixed oxides prepared by Zr^{4+} and Ti^{4+} chlorides precipitation in basic media [6]. Low-temperature solvo-treatment provoked further increase in ZrO_2 surface concentration. Thus, surface composition of Mo(2.8)/ZTSL4 became nearly equimolar. The higher Lewis acidity of this oxide (Fig. 6) could be related to these strong changes in surface composition.

Figs. 14 and 15 show the deconvoluted Mo 3d spectra for Mo(2.8)/ZT and Mo(2.8)/ZTSL4, respectively. In the former, the Mo 3d doublet could be satisfactorily fitted by considering Mo^{4+} (from MoS_2) and Mo^{5+} (from molybdenum oxy-sulfides), the corresponding proportions being 81 and 19%, respectively. Surprisingly, molybdenum in the highest oxidation state had to be taken into account (Mo^{6+}) to adequately fit the Mo 3d peak for Mo(2.8)/ZTSL4, while the Mo^{5+} proportion remained essentially unchanged as compared with the previous solid (ca. 18%). The existence of Mo^{6+} species (about 8%) suggests that ZTSL4 promoted stronger Mo-support interaction than ZT, preventing sulfiding to a higher extent. This fact clearly

Table 4
Composition of MoS_2 catalysts supported on ZrO_2–TiO_2 (Zr/Ti = 30/70 nominal molar ratio) oxides solvo-treated at 353 K

Sample	Mo[a] (wt.%)	Mo[b] (wt.%)	Zr/Ti[a] (mol ratio)	Zr/Ti[b] (mol ratio)	Zr/Ti[c] (mol ratio)
Mo(2.8)/ZT	11.45	11.28	3/7	2.97/7	4.86/7
Mo(2.8)/ZTSL1	13.10	11.54	3/7	2.8/7	–
Mo(2.8)/ZTSL4	12.35	10.76	3/7	3.7/7	6.54/7

That impregnated on non-solvo-treated oxide included as reference.
[a] Nominal composition.
[b] Bulk composition (by ICP).
[c] Surface composition (by XPS).

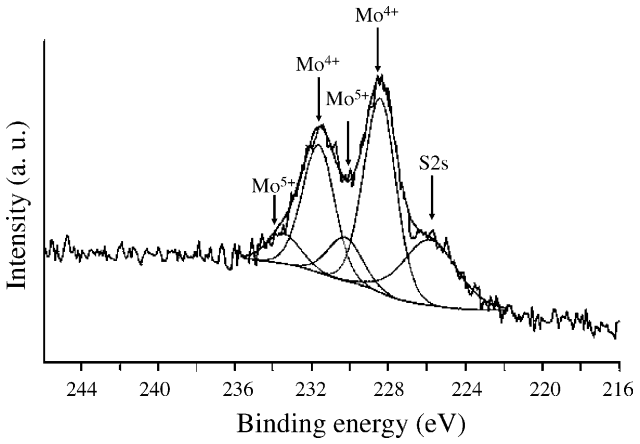

Fig. 14. XPS spectra of sulfided Mo(2.8) on non-solvotreated ZrO_2–TiO_2 (Zr/Ti = 30/70 nominal molar ratio).

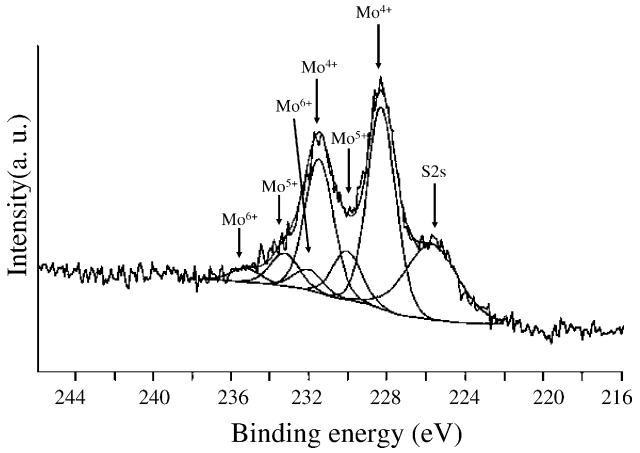

Fig. 15. XPS spectra of sulfided Mo(2.8) on ZrO_2–TiO_2 (Zr/Ti = 30/70 nominal molar ratio) solvo-treated at 353 K (4 days).

indicated that the active phase state was different on each support. It could be that the much more acidic surface of the solvo-treated oxide could influence sulfiding and, as aforementioned, supported molybdenum sulfide dispersion. Nevertheless, with the information available no further discussion could be made. MoS_2 dispersion could not be estimated from the I_{Mo}/I_{Zr} and I_{Mo}/I_{Ti} XPS peaks ratio considering the different surface composition of the used supports. Deeper characterization is needed to shed light on the observed behavior.

4. Conclusions

Solvo-treatment of alcogels obtained by low-temperature (273 K) acid-catalyzed hydrolysis of Zr and Ti alkoxides resulted very useful in obtaining mixed oxides of tailor-made textural properties. Solvo-treatment at low temperature (353 K) for 1 day was specially suitable to produce materials of improved properties as HDS catalyst support due to its high surface area, high porosity, average pore size (∼9 nm) and increased Lewis acidity. Wider pores (>22 nm) but much lower S_g (∼70–80 $m^2\,g^{-1}$) were observed when solvo-treatment was carried out at 513 K. The high-temperature solvo-treated samples produced solids of acidity-free surface that proved to be detrimental on catalyst stability. MoS_2 catalysts (at 2.8 Mo atoms nm^{-2}) supported on binary oxides solvo-treated at 353 K showed increased activity by a factor of ca. 3 in DBT HDS, as compared to that on conventional ZrO_2–TiO_2. Highly-loaded catalyst (5.6 Mo atoms nm^{-2}) had decreased activity, probably due to lower MoS_2 dispersion. At a given loading lower sulfiding degree was observed for ZTSL4-supported catalyst, as to that of Mo/ZT. This could be probably originated in different Mo-support interaction due to changes in surface composition provoked by low-temperature solvo-treatment. Lewis acidity appeared to play a decisive role on HDS performance, probably by influencing both Mo sulfiding and dispersion.

Acknowledgements

The authors recognize financial support from Instituto Mexicano del Petróleo (FIES 98-117-II D.0090 grant). María C. Barrera is also indebted to CONACYT for a graduate student scholarship (95326).

References

[1] B.M. Reddy, P.M. Sreekanth, Y. Yamada, Q. Xu, T. Kobayashi, Appl. Catal. A 228 (2002) 269.
[2] G. Colón, M.C. Hidalgo, J.A. Navío, Appl. Catal. A 231 (2002) 185.
[3] H.-R. Chen, J.-L. Shi, J. Yu, L.-Z. Wang, D.-S. Yan, Microporous Mesoporous Mater. 39 (2000) 171.
[4] S.K. Maity, M.S. Rana, S.K. Bej, J. Ancheyta, G. Murali Dhar, Catal. Lett. 72 (1–2) (2001) 115.
[5] C.-M. Lu, Y.-M. Lin, I. Wang, Appl. Catal. A 198 (2000) 223.
[6] F.P. Daly, H. Ando, J.L. Schmitt, E.A. Sturm, J. Catal. 108 (1987) 401.
[7] F.P. Daly, H. Ando, H.C. Foley, H.J. Jung, US Patent 5,021,385 (1991).
[8] F.P. Daly, J. Catal. 116 (1989) 600.
[9] J.G. Weissman, E.I. Ko, S. Kaytal, Appl. Catal. A 94 (1993) 45.
[10] D.J. Suh, T.J. Park, H.Y. Han, J.Ch. Lim, Chem. Mater. 14 (2002) 1452.
[11] O. Metelkina, N. Hüsing, P. Pongratz, U. Schubert, J. Non-Cryst. Solids 285 (2001) 64.
[12] M.C. Barrera, M. Viniegra, J. Escobar, J.A. De Los Reyes, 18th NACS Meeting, Cancún, Q. Roo, México, 1–6 June 2003. Technical Program, p. 78.
[13] Y. Yue, X. Zhao, W. Hua, Z. Gao, Appl. Catal. B 46 (2003) 561.
[14] W.W. So, S.B. Park, K.J. Kim, Ch.H. Shin, S.J. Moon, J. Mater. Sci. 36 (2001) 4299.
[15] K. Yanagisawa, J. Ovenstone, J. Phys. Chem. B 103 (1999) 7781.
[16] Ch.Ch. Wang, J.Y. Ying, Chem. Mater. 11 (1999) 3113.
[17] M. Wu, G. Lin, D. Chen, G. Wang, D. He, Sh. Feng, R. Xu, Chem. Mater. 14 (2002) 1974.
[18] C. Lahousse, A. Aboulayt, F. Maugé, J. Bachelier, J.C. Lavalley, J. Mol. Catal. 94 (1993) 283.
[19] M.C. Barrera, J. Escobar, C. Marín, M. Viniegra, J.A. De Los Reyes, J.G. Pacheco, F. Murrieta, Pet. Sci. Technol. 22 (1–2) (2004) 87.

[20] R. Bacaud, D. Letourneur, J.J. Lecomte, M. Vrinat, in: Proceedings of the 16th Simp. Iber. Cat., Cartagena, Col., 1998, p. 67.
[21] J.M. Miller, L.J. Lakshmi, J. Phys. Chem. B 102 (1998) 6465.
[22] L.L. Hench, J.K. West, Chem. Rev. 90 (1990) 33.
[23] Q. Xu, M.A. Anderson, J. Am. Ceram. Soc. 76 (8) (1993) 2093.
[24] A.E. McHale, R.S. Roth, J. Am. Ceram. Soc. 69 (11) (1986) 827.
[25] I. Wang, R.-Ch. Chang, J. Catal. 117 (1989) 266.
[26] H. Zou, Y.S. Lin, Appl. Cat. A 265 (2004) 35.
[27] R. Barthos, F. Lónyi, J. Engelhardt, J.A. Valyon, Top. Catal. 10 (2000) 79.
[28] H-R. Chen, J.-L. Shin, J. Yu, L.-Z. Wang, D.-S. Yan, Microporous Mesoporous Mater. 39 (2000) 171.
[29] K. Kosuge, P.S. Singh, J. Phys. Chem. B 103 (1999) 3563.
[30] L. Mosqueira, G.A. Fuentes, Mol. Phys. 100 (9) (2002) 3055.
[31] R.S. Weber, J. Catal. 151 (1995) 470.
[32] J. Ramírez, L. Cedeño, G. Busca, J. Catal. 184 (1999) 59.
[33] J. Ramírez, L. Ruiz, L. Cedeño, V. Harlé, M. Vrinat, M. Breysse, Appl. Catal. 93 (1993) 163.
[34] X. Xu, P. Waller, E. Crezee, Z. Shan, F. Kapteijn, J.A. Moulijn, Stud. Surf. Sci. Catal. 143 (2002) 1019.
[35] S. Dzwigaj, C. Louis, M. Breysse, M. Cattenot, V. Belliere, C. Geantet, M. Vrinat, P. Blanchard, E. Payen, S. Inoue, H. Kudo, Y. Yoshimura, Appl. Catal. B 41 (2003) 181.
[36] M. Houalla, N. Nag, A.V. Sapre, D.H. Broderick, B.C. Gates, AIChE J. 24 (6) (1978) 1015.
[37] M. Daage, R.R. Chianelli, J. Catal. 149 (1994) 414.
[38] J. Mijoin, G. Pérot, F. Bataille, J.L. Lemberton, M. Breysse, S. Kasztelan, Catal. Lett. 71 (3–4) (2001) 139.
[39] E.J.M. Hensen, P.J. Kooyman, Y. van der Meer, A.M. van der Kraan, V.H.J. de Beer, J.A.R. van Veen, R.A. van Santen, J. Catal. 199 (2001) 224.